

A dynamical theory of extremely asymmetric x-ray diffraction taking account of normal lattice strain

S Stepanov† and R Köhler

MPG-AG 'Röntgenbeugung', Hausvogteiplatz 5–7, D-10117 Berlin, Germany

Abstract. An approach is described to compute extremely asymmetric x-ray diffraction in multilayers and superlattices taking account of the normal lattice strain. This method is based on the dynamical theory of x-ray diffraction and on a matrix form of boundary conditions, thus providing a simple numerical solution to the problem. The developed approach can be used to interpret extremely asymmetric x-ray diffraction measurements of lattice strains in semiconductor multilayers and in other surface structures.

1. Introduction

Dynamical x-ray diffraction is a well known technique for studying tiny distortions and lattice strains in perfect crystals. However, this method is only applicable to those cases in which the strained layers are thicker than, or of the same order as, the x-ray extinction length, which is usually 1–10 μm [1,2]. In recent years this scale of depth has become too crude for many applications, especially for modern microelectronics, with strained layers being often as thin as 10^{-3} – 10^{-2} μm .

The extinction length can be decisively shortened if x-ray diffraction is combined with grazing incidence or grazing exit of x-rays with respect to the crystal surface [3]. In this case the extinction length is reduced to 10^{-3} – 10^{-2} μm due to evanescent waves caused by the total external reflection effect. Maximum sensitivity to thin layers is attained with both grazing incidence and exit [4–6]. This case is usually referred to as the grazing-incidence diffraction scheme (GID). However, GID does not provide any information about lattice spacing along the crystal surface normal because the diffraction vector runs parallel to the surface. Therefore, it is only possible to measure changes in lateral lattice spacing. However, there is no change in lateral lattice spacing in thin layers, unless there are misfit dislocations.

Thus, the extremely asymmetric x-ray diffraction (XEAD) technique, with either grazing incidence or grazing exit, is likely to elicit great interest in application since it combines sensitivity to thin surface layers with the opportunity to measure normal lattice strain.

The theory of x-ray diffraction under total external reflection conditions for perfect (unstrained) crystals has been put forward in many papers [4, 6–10]. However, for

layers with variable lattice spacing the situation is less clear since the Takagi–Taupin equations are inapplicable. The reason is that x-ray wavefield amplitudes are inclined to vary at a depth scale that is comparable to interatomic distances and, hence, the second derivatives of wavefield amplitudes in the Maxwell equations cannot be disregarded. Moreover, specular reflection and refraction effects should be included in the boundary conditions by analogy with the perfect crystal case. The matrix extension of the Takagi–Taupin equations, as suggested in [11, 11a] is generally applicable, but lattice strain has not been included in this model. Additionally, a numerical solution to matrix Takagi–Taupin equations is highly complicated and may turn out to be unstable for the sharp interfaces in multilayers due to the assumption that wavefunctions and their derivatives are smooth.

In the present paper we put forward a simple and physically persuasive approach to computing GID and XEAD in multilayers under normal strain. The algorithm suggested is based on the extended dynamical diffraction theory, taking due consideration of the specular reflection and refraction effects. It is held to be an extension of the matrix solution to GID in multilayers, as recently published in [12]. The approach used in [12] was essentially the same, but strain effects were not taken into account.

Section 2 deals with the derivation of the equations for the general case, including both GID and XEAD. Section 3 discusses simplification of the general formulae for XEAD, with either grazing incidence or grazing exit. Section 4 supplements the algorithm with formulae simulating various experimental scans. This section was included since modelling of non-coplanar XEAD geometry poses a special problem that is not trivial. Finally, section 5 provides numerical examples and discusses the advantages of XEAD in studying lattice strains in thin layers.

† Permanent address: Institute for Nuclear Problems, 11 Bobruiskaya St, SU-220050 Minsk, Republic of Belarus.

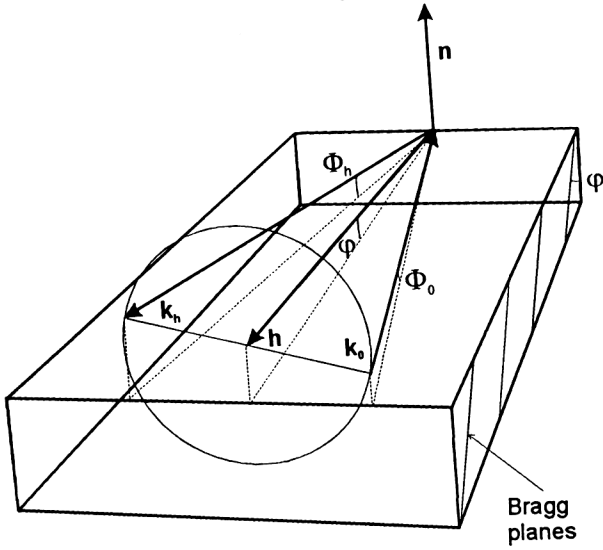


Figure 1. Schematic view of extremely asymmetric x-ray diffraction. For explanations see text.

2. Derivation of basic equations

Let us consider GID or XEAD in a multilayered structure that is composed of N crystalline layers with matched lateral spacing: $\mathbf{h}_{\parallel}^i = \mathbf{h}_{\parallel}^j = \dots \equiv \mathbf{h}_{\parallel}$, $h_z^i \neq h_z^j \neq \dots$ (\mathbf{h}^i is the reciprocal lattice vector of Bragg diffraction in the i th layer, \mathbf{h}_{\parallel} and h_z denote lateral and normal components respectively). Those structures that contain additional amorphous layers are not considered here for reasons of simplicity. Nevertheless, the amorphous layers can be readily included in the model by analogy with [12].

Let \mathbf{k}_0 be the wavevector of the incident wave and \mathbf{k}_h that of the diffracted wave in vacuum above the crystal surface (figure 1). The salient point is that despite different lattice spacings in layers only one diffracted wave leaves the crystal. Since $\mathbf{k}_{h\parallel} = \mathbf{k}_{0\parallel} + \mathbf{h}_{\parallel}$ applies to all layers, the normal components of the diffracted waves in vacuum connected with different layers are proven to be the same due to retention of the x-ray wavelength. Thus, all waves leave the crystal at the same angle $\Phi_h = \arcsin(k_{hz}/k_0) = \arcsin[(k_0^2 - k_{h\parallel}^2)^{1/2}/k_0]$.

This effect noted earlier in the kinematical analysis of problem [13] will not be sustained if there is a lateral mismatch in the lattice spacings [14].

Thus, in a general case, the wavefield in vacuum for every incident x-ray polarization consists of three waves (incident, specularly reflected and diffracted waves):

$$\begin{aligned} E_v(\mathbf{r}) = & E_0 \exp(ik_0\gamma_0 z) \exp(i\mathbf{k}_{0\parallel} \cdot \mathbf{r}_{\parallel}) \\ & + E_s \exp(-ik_0\gamma_0 z) \exp(i\mathbf{k}_{0\parallel} \cdot \mathbf{r}_{\parallel}) \\ & + E_h \exp(-ik_0\gamma_h z) \exp[i(\mathbf{k}_0 + \mathbf{h})_{\parallel} \cdot \mathbf{r}_{\parallel}] \end{aligned} \quad (1)$$

Here $\gamma_{0,h} = \mathbf{k}_{0,h} \cdot \mathbf{n} / k_0 = \sin \Phi_{0,h}$; the vector \mathbf{n} is the unit vector along the internal crystal surface normal, Φ_0 is the incidence glancing angle, Φ_h is the exit angle of the diffracted wave, E_0 , E_s and E_h are the amplitudes of the x-ray waves.

The x-ray wavefield inside every k th crystalline layer consists of four pairs of diffracted and transmitted waves

$$\begin{aligned} D^k(\mathbf{r}) = & \sum_{j=1}^4 D_{0j}^k \exp(ik_0 u_j^k z) \exp(i\mathbf{k}_{0\parallel} \cdot \mathbf{r}_{\parallel}) \\ & + \sum_{j=1}^4 D_{hj}^k \exp[ik_0(u_j^k + \psi^k)z] \exp[i(\mathbf{k}_0 + \mathbf{h})_{\parallel} \cdot \mathbf{r}_{\parallel}] \end{aligned} \quad (2)$$

where D_{0j}^k and D_{hj}^k are the amplitudes of these waves that are interrelated with the dynamical diffraction equations

$$D_{hj}^k = \frac{u_j^k{}^2 - \gamma_0^2 - \chi_0^k}{\chi_h^k} D_{0j}^k \equiv V_j^k D_{0j}^k \quad j = 1, 2, 3, 4 \quad (3)$$

and the parameters u_j^k are the solutions of the respective fourth-order dispersion equation

$$(u_j^k{}^2 - \gamma_0^2 - \chi_0^k) [(u_j^k + \psi^k)^2 - \gamma_h^2 - \chi_0^k] = \chi_h^k \chi_0^k. \quad (4)$$

The quantities χ_0^k , χ_h^k and χ_{\parallel}^k are the Fourier components of x-ray dielectric susceptibility in the k th layer; $\psi^k = \mathbf{h}^k \cdot \mathbf{n} / k_0 = 2 \sin \theta_B^k \sin \varphi^k$, φ^k are the angles between \mathbf{h}^k and the surface, θ_B^k are the Bragg angles.

As shown in [15], there are always two solutions of (4) with $\text{Im } u_j^k > 0$ and 2 solutions with $\text{Im } u_j^k < 0$. Inside the crystal the exponentials in (2) are damped for the former roots and raised for the latter. The roots with $\text{Im } u_j^k < 0$ are non-physical for the infinitely thick bottom layer (the substrate) of the structure because they provide infinitely rising exponentials. Therefore, only two pairs of wavefields D_{01}^N, D_{h1}^N and D_{02}^N, D_{h2}^N remain in the substrate.

In order to find the x-ray amplitudes E_s , E_h , D_0^1, \dots, D_0^N the boundary conditions for x-ray wavefields and their derivatives at all interfaces should be used. These conditions can be represented in the form (see [12] for more details):

$$\begin{aligned} E_0 + E_s &= \sum_{j=1}^4 D_j^1 \\ E_h &= \sum_{j=1}^4 V_j^1 D_j^1 \\ \gamma_0(E_0 - E_s) &= \sum_{j=1}^4 u_j^1 D_j^1 \\ -\gamma_h E_h &= \sum_{j=1}^4 w_j^1 D_j^1 \end{aligned} \quad (5)$$

at the vacuum–crystal interface, and

$$\begin{aligned}
 \sum_{j=1}^4 f_j^{k(L)} D_j^k &= \sum_{j=1}^M f_j^{k+1(U)} D_j^{k+1} \\
 \sum_{j=1}^4 V_j^k f_j^{k(L)} D_j^k g^{k(L)} &= \sum_{j=1}^M V_j^{k+1} f_j^{k+1(U)} D_j^{k+1} g^{k+1(U)} \\
 \sum_{j=1}^4 u_j^k f_j^{k(L)} D_j^k &= \sum_{j=1}^M u_j^{k+1} f_j^{k+1(U)} D_j^{k+1} \\
 \sum_{j=1}^4 w_j^k f_j^{k(L)} D_j^k g^{k(L)} &= \sum_{j=1}^M w_j^{k+1} f_j^{k+1(U)} D_j^{k+1} g^{k+1(U)}
 \end{aligned} \tag{6}$$

at the interface between two crystalline layers. Here $M = 2$ for $k = N - 1$ and $M = 4$ for the other layers. The following notations are also used:

$$\begin{aligned}
 w_j^k &= V_j^k (u_j^k + \psi^k) & f_j^k &= \exp(iu_j^k k_0 z) \\
 g^k &= \exp(i\psi^k k_0 z).
 \end{aligned}$$

Indices (L) and (U) indicate that the respective exponent is evaluated at the lower (upper) boundary of the layer. Apparently, $(L)_k = (U)_{k+1}$.

Equations (5) and (6) can be rewritten in a matrix form if the following matrices and vectors are introduced:

$$\begin{aligned}
 \mathbf{E}^v &= (E_0 \equiv 1, E_{0h} \equiv 0, E_s, E_h) \\
 \mathbf{D}^k &= (D_{01}^k, D_{02}^k, D_{03}^k, D_{04}^k)
 \end{aligned} \tag{7}$$

$$\begin{aligned}
 \mathbf{S}^v &= \begin{pmatrix} 1 & 0 & 1 & 0 \\ 0 & 1 & 0 & 1 \\ \gamma_0 & 0 & -\gamma_0 & 0 \\ 0 & \gamma_h & 0 & -\gamma_h \end{pmatrix} \\
 \mathbf{S}^k &= \begin{pmatrix} 1 & 1 & 1 & 1 \\ V_1^k & V_2^k & V_3^k & V_4^k \\ u_1^k & u_2^k & u_3^k & u_4^k \\ w_1^k & w_2^k & w_3^k & w_4^k \end{pmatrix}
 \end{aligned} \tag{8}$$

$$\mathbf{A}^k = \mathbf{G}^{k(U)} \mathbf{S}^k \mathbf{F}^{k(U)} \quad \mathbf{B}^k = \mathbf{G}^{k(L)} \mathbf{S}^k \mathbf{F}^{k(L)} \tag{9}$$

where $F_{ij}^k = f_i^k \delta_{ij}$ and $G_{ij}^k = \zeta_i^k \delta_{ij}$ are diagonal square matrices, $\zeta_1^k = \zeta_3^k = 1$, and $\zeta_2^k = \zeta_4^k = g^k$. For $k = 1, \dots, N - 1$ the size of all matrices is (4×4) . In the case of the substrate layer the matrix \mathbf{F}^N is (2×2) and \mathbf{S}^N is (2×4) since only two roots with $\text{Im } u_j^k > 0$ are taken into account.

Substituting (7)–(9) into (5) and (6) we obtain

$$\begin{aligned}
 \mathbf{S}^v \mathbf{E}^v &= \mathbf{A}^1 \mathbf{D}^1 \\
 \mathbf{B}^1 \mathbf{D}^1 &= \mathbf{A}^2 \mathbf{D}^2 \\
 &\vdots \\
 \mathbf{B}^k \mathbf{D}^k &= \mathbf{A}^{k+1} \mathbf{D}^{k+1} \\
 &\vdots \\
 \mathbf{B}^{N-1} \mathbf{D}^{N-1} &= \mathbf{A}^N \mathbf{D}^N.
 \end{aligned} \tag{10}$$

This is the matrix form of boundary conditions. Carrying out the substitution for every line in (10) up to the upper one we arrive at

$$\begin{aligned}
 \mathbf{E}^v &= (\mathbf{S}^v)^{-1} \mathbf{A}^1 (\mathbf{B}^1)^{-1} \\
 &\times \dots \mathbf{A}^{N-1} (\mathbf{B}^{N-1})^{-1} \mathbf{A}^N \mathbf{D}^N \equiv \tilde{\mathbf{S}} + \mathbf{D}^N
 \end{aligned} \tag{11}$$

where $\tilde{\mathbf{S}}$ is a (2×4) matrix and (11) is a set of four linear algebraic equations with respect to four variables: E_s, E_h, D_{01}^N and D_{02}^N . The solution for E_h is

$$E_h = \frac{\tilde{S}_{41} \tilde{S}_{22} - \tilde{S}_{42} \tilde{S}_{21}}{\tilde{S}_{11} \tilde{S}_{22} - \tilde{S}_{12} \tilde{S}_{21}} \tag{12}$$

and the reflection coefficient is calculated according to the formula

$$P_h = (\text{Re } \gamma_h / \gamma_0) |E_h|^2. \tag{13}$$

Obviously, equation (13) provides the solution to the problem in principle. However, the parameter γ_h and the matrix $\tilde{\mathbf{S}}$ need to be evaluated.

The equation for γ_h derived in [15] is

$$\gamma_h^2 = (\gamma_0 + \psi^k)^2 - \alpha_k \tag{14}$$

with $\alpha_k = [(\mathbf{k}_0 + \mathbf{h})^2 - k_0^2] / k_0^2$ being the parameter describing deviation of the incident wave from the exact Bragg condition. It is easy to show that in our case, γ_h does not depend on k :

$$\begin{aligned}
 \gamma_h^2 &= (\gamma_0 + \psi^k)^2 - \alpha_k = \frac{(\mathbf{k}_0 \cdot \mathbf{n} + \mathbf{h} \cdot \mathbf{n} + \Delta h^k)^2}{k_0^2} \\
 &- \frac{(\mathbf{k}_0 + \mathbf{h} + \Delta h^k \mathbf{n})^2}{k_0^2} = (\gamma_0 + \psi)^2 - \alpha
 \end{aligned}$$

where ψ and α are the mean parameters and Δh^k are the deviations of \mathbf{h}^k from the mean value in different layers: $\mathbf{h}^k = \mathbf{h} + \Delta h^k \mathbf{n}$.

Consider now the structure of the matrix $\tilde{\mathbf{S}}$:

$$\begin{aligned}
 \tilde{\mathbf{S}} &= (\mathbf{S}^v)^{-1} \mathbf{S}^1 \mathbf{F}^{1(U)} (\mathbf{F}^{1(L)})^{-1} (\mathbf{S}^1)^{-1} (\mathbf{G}^{1(L)})^{-1} \\
 &\times \mathbf{G}^{2(U)} \mathbf{S}^2 \mathbf{F}^{2(U)} \dots \mathbf{G}^{N(U)} \mathbf{S}^N \mathbf{F}^{N(U)}.
 \end{aligned} \tag{15}$$

Equation (15) can be re-written as a product of transmittancy matrices \mathbf{T}^k introduced in [12] and ‘strain’ matrices $\hat{\mathbf{G}}^{k,k+1}$:

$$\tilde{\mathbf{S}} = (\mathbf{S}^v)^{-1} \mathbf{T}^1 \hat{\mathbf{G}}^{1,2} \mathbf{T}^2 \hat{\mathbf{G}}^{2,3} \dots \mathbf{T}^{N-1} \hat{\mathbf{G}}^{N-1,N} \mathbf{S}^N \mathbf{F}^{N(U)} \tag{16}$$

where:

$$\mathbf{T}^k = \mathbf{S}^k \mathbf{F}^{k(U)} (\mathbf{F}^{k(L)})^{-1} (\mathbf{S}^k)^{-1} = \mathbf{S}^k \hat{\mathbf{F}}^k (\mathbf{S}^k)^{-1} \tag{17}$$

$$\hat{\mathbf{G}}^{k,k+1} = (\mathbf{G}^{k(L)})^{-1} \mathbf{G}^{k+1(U)}. \tag{18}$$

Matrices $(\hat{\mathbf{F}}^k)_{ij} = \exp(-iu_j^k k_0 t^k) \delta_{ij}$ are diagonal matrices containing the phase changes of the x-ray waves on the path from upper to lower layer interfaces. The parameters $t^k = z^{k(L)} - z^{k(U)}$ are the thicknesses of layers.

If the thickness of a layer tends to zero, then: $\hat{\mathbf{F}}^k \rightarrow \mathbf{I}$, and $\mathbf{T}^k \rightarrow \mathbf{S}^k(\mathbf{S}^k)^{-1} = \mathbf{I}$. Thus, the T matrix of an infinitely thin layer tends to a diagonal unit matrix and the effect of the layer disappears.

The matrices

$$(\hat{G}^k)_{ij} = \exp[ik_0 z^{k,k+1}(\zeta_i^{k+1} - \zeta_i^k)]\delta_{ij}$$

describe the effect of change in the normal lattice spacing from layer to layer. The parameters ψ^k can be represented in the form

$$\psi^k = \psi(1 + \Delta a_z^k/a_z) \quad (19)$$

and the exponents for $G_{22}^{k,k+1}$ and $G_{44}^{k,k+1}$ can be written as

$$k_0 z \psi \Delta a_z^{k+1,k}/a_z = h_z z \Delta a_z^{k+1,k}/a_z \quad (20)$$

The right-hand side of (20) contains the well-known term that describes the effect of the normal lattice strain on Bragg diffraction. In the absence of the strain ($\hat{\mathbf{G}}^k = \mathbf{I}$), and the equation for $\hat{\mathbf{S}}$ is reduced to that obtained in [13].

Thus, computation of the matrix $\tilde{\mathbf{S}}$ for an arbitrary strain gradient in crystal multilayers is straightforward. The derived equations are general on the understanding that they are valid for both GID and XEAD.

3. Reduction of equations in XEAD cases

The equations presented in the previous section can be considerably simplified if either the incident or the diffracted beam makes a large angle with respect to the crystal surface, because in this case the specular reflection effect is negligible for the non-grazing beam.

Theoretical analysis pertaining to XEAD in perfect crystals was carried out in [16]. As shown in [16], the dispersion equation (4) for XEAD becomes a third-order one and only three wavefields are excited in every layer. Besides, the boundary conditions for the wavefields derivatives can be dropped for non-grazing waves.

Basically, the approximate analytical solutions of dispersion equation (4) were obtained for XEAD with grazing exit [17] and grazing incidence [18]. These solutions can be used in every crystalline layer with the matrix form of boundary conditions, as derived in the previous section. However, when a computer is always employed for matrix transformations, the numerical solutions are preferable because they are more accurate.

Below are presented the results on reduction of the general formulae for grazing incidence and grazing exit XEAD.

3.1. Grazing incidence

The approximate dispersion equation is (see [16] for details)

$$(u^2 - \gamma_0^2 - \chi_0)[u + \psi + (\gamma_h^2 + \chi_0)^{1/2}] = -\frac{\chi_h \chi_{\bar{h}}}{2\gamma_h} \quad (21)$$

This equation has one solution corresponding to the wavefield damping inside the crystal and two solutions corresponding to the rising wavefields.

The boundary conditions can be simplified since the conditions for the derivatives of diffracted waves can be discarded. Equally, the matrices in (7)–(9) are reduced to the form

$$\begin{aligned} \mathbf{E}^v &= (1, E_s, E_h) \\ \mathbf{D}^k &= (D_{01}^k, D_{02}^k, D_{03}^k) \end{aligned} \quad (22)$$

$$\mathbf{S}^v = \begin{pmatrix} 1 & 1 & 0 \\ \gamma_0 & -\gamma_0 & 0 \\ 0 & 0 & 1 \end{pmatrix} \quad \mathbf{S}^k = \begin{pmatrix} 1 & 1 & 1 \\ u_1^k & u_2^k & u_3^k \\ V_1^k & V_2^k & V_3^k \end{pmatrix} \quad (23)$$

$$\hat{\mathbf{G}}^{k,k+1} = \begin{pmatrix} 1 & 0 & 0 \\ 0 & 1 & 0 \\ 0 & 0 & \hat{g}^{k,k+1} \end{pmatrix} \quad (24)$$

where we have designated $\hat{g}^{k,k+1} = \exp[i(\psi^{k+1} - \psi^k)k_0 z^{k,k+1}]$.

In the substrate layer only one solution D_{01}^N corresponding to the dampened x-ray wavefield has to be taken into account and therefore \mathbf{S}^N is reduced to a (1×3) matrix. After evaluation of $\tilde{\mathbf{S}}$ according to (16) the solution to the diffracted wave can be obtained in the form

$$E_h = \tilde{S}_{31}/\tilde{S}_{11} \quad (25)$$

3.2. Grazing exit

In this case the dispersion equation is also of third order [17],

$$(u''^2 - \gamma_h^2 - \chi_0)[u'' - \psi - (\gamma_0^2 + \chi_0)^{1/2}] = \frac{\chi_h \chi_{\bar{h}}}{2\gamma_0} \quad (26)$$

where $u = u'' - \psi$. However, unlike (21), this equation provides two solutions corresponding to damped wave amplitudes and one corresponding to waves with rising amplitudes.

Since the incident wave in vacuum and the transmitted waves in the crystal make large angles with the surface, the boundary conditions for their derivatives can be discarded. The specularly reflected wave in vacuum can for the same reason also be neglected. Consequently, the matrices in (7)–(9) can be simplified to

$$\begin{aligned} \mathbf{E}^v &= (1, 0, E_h) \\ \mathbf{D}^k &= (D_{01}^k, D_{02}^k, D_{03}^k) \end{aligned} \quad (27)$$

$$\mathbf{S}^v = \begin{pmatrix} 1 & 0 & 0 \\ 0 & 1 & 1 \\ 0 & \gamma_h & -\gamma_h \end{pmatrix} \quad \mathbf{S}^t = \begin{pmatrix} 1 & 1 & 1 \\ V_1^k & V_2^k & V_3^k \\ w_1^k & w_2^k & w_3^k \end{pmatrix} \quad (28)$$

$$\hat{\mathbf{G}}^{k,k+1} = \begin{pmatrix} 1 & 0 & 0 \\ 0 & \hat{g}^{k,k+1} & 0 \\ 0 & 0 & \hat{g}^{k,k+1} \end{pmatrix}. \quad (29)$$

In the substrate layer two damped wavefields D_{01}^N and D_{02}^N are taken into account since (26) has two roots with $\text{Im } u_j^k > 0$. Therefore, the matrices \mathbf{S}^N and $\tilde{\mathbf{S}}$ are of size (2×3) . After evaluation of $\tilde{\mathbf{S}}$ the solution for E_h can be found in the following form:

$$E_h = \frac{\tilde{S}_{31}\tilde{S}_{22} - \tilde{S}_{32}\tilde{S}_{21}}{\tilde{S}_{11}\tilde{S}_{22} - \tilde{S}_{12}\tilde{S}_{21}}. \quad (30)$$

In general, application of the outlined approximate solutions provides more than a two-fold gain in computation rate.

4. Simulation of XEAD measurements

The formulae derived in the previous sections provide the computation of GID and XEAD depending on two diffraction angles Φ_0 and Φ_h , where Φ_h is connected through equation (14) with the incident beam position parameter α . As the XEAD experiments are basically non-coplanar (that is, the plane formed by the incident and diffracted waves need not be perpendicular to the crystal surface), evaluation of α and Φ_h presents a special problem.

The numerical solution to this problem consists of several steps.

4.1. Determination of the crystal surface normal

Let \mathbf{b} be the basic surface normal (such as (100), (110), ... and so on), δ the maximum misorientation angle of the real surface normal \mathbf{n} with respect to \mathbf{b} and \mathbf{r} be the reference vector specifying the direction of maximum misorientation (such as (001), $(1\bar{1}0)$, ...). These parameters are usually known from the experiment. To determine the vector \mathbf{n} one can represent it in the form

$$\mathbf{n} = c_1\mathbf{b} + c_2\mathbf{r} \quad (31)$$

where the coefficients c_1 and c_2 can be evaluated with the help of the conditions $n^2 = 1$ and $\mathbf{n} \cdot \mathbf{b} = \cos \delta$.

4.2. Determination of the incident wavevector

It is assumed that at least one of the angles Φ_0 or Φ_h can be measured at the exact Bragg position of the incident beam in the experiment. Usually, a small grazing angle is measured. Let this angle be Φ_0 , for certainty. Then, the incident wavevector \mathbf{k}_0 can be written as

$$\mathbf{k}_0 = c_1\mathbf{k}_0\mathbf{n} + c_2\mathbf{h} + c_3(\mathbf{h} \times \mathbf{n}) \quad (32)$$

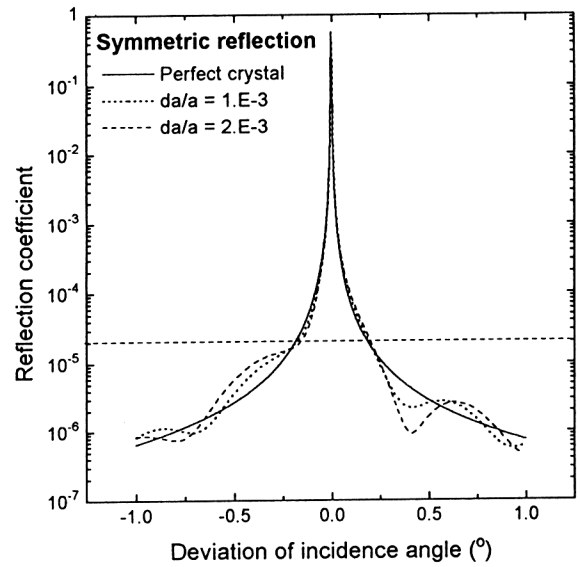


Figure 2. The effect of a 100 Å strained surface layer on symmetric Bragg reflection.

where the coefficients c_1 , c_2 and c_3 can be determined using the following conditions:

$$\begin{aligned} \mathbf{k}_0 \cdot \mathbf{n} &= k_0 \sin \Phi_0 = k_0(c_1 + c_2 \psi) \\ \mathbf{k}_0 \cdot \mathbf{h} &= -k_0 h \sin \theta_B = k_0^2(c_1 \psi + 4c_2 \sin^2 \theta_B) \\ \mathbf{k}_0^2 &= k_0^2 = c_1^2 k_0^2 + c_2^2 h^2 + c_3^2 (\mathbf{h} \times \mathbf{n})^2 + 2c_1 c_2 k_0^2 \psi. \end{aligned} \quad (33)$$

4.3. Simulation of measurement scans

The scans in x-ray experiments are always rotations of the incident x-ray vector around some axis. Therefore, it is possible to write

$$\mathbf{k}_0 = \mathbf{k}_0^{\text{Br}} + k_0 \mathbf{a} \Theta \quad (34)$$

where \mathbf{a} is a unit vector satisfying the condition $\mathbf{k}_0 \cdot \mathbf{a} = 0$, Θ is the scanning angle measured in the experiment and \mathbf{k}_0^{Br} is the exact Bragg position vector evaluated according to (32).

As shown in [19], the parameter α can be expressed via \mathbf{a} and Θ as follows:

$$\alpha = 2\Theta(\mathbf{a} \cdot \mathbf{h})/k_0 + 2\Theta^2 \sin^2 \theta_B. \quad (35)$$

Then, the parameter γ_h can be found according to (14) which can be conveniently rewritten as

$$\gamma_h^2 = (\gamma_h^{\text{Br}} + \Delta\gamma_0)^2 - \alpha \quad (36)$$

where $\Delta\gamma_0 = \Theta(\mathbf{a} \cdot \mathbf{n})$, and $\gamma_h^{\text{Br}} = \gamma_0^{\text{Br}} + \psi$ is plus/minus the value of γ_h at the exact Bragg position.

The formulae presented above have been included in our computer program. Although the direction of \mathbf{a} is restricted only by the condition $\mathbf{k}_0 \cdot \mathbf{a} = 0$, it is, in the experiments, usually chosen along one of the following directions: $[\mathbf{k}_0 \times \mathbf{n}]$, $[\mathbf{k}_0 \times \mathbf{h}]$, $[\mathbf{k}_0 \times [\mathbf{k}_0 \times \mathbf{n}]]$ or $[\mathbf{k}_0 \times [\mathbf{k}_0 \times \mathbf{h}]]$. Examples of the computations are given in section 5.

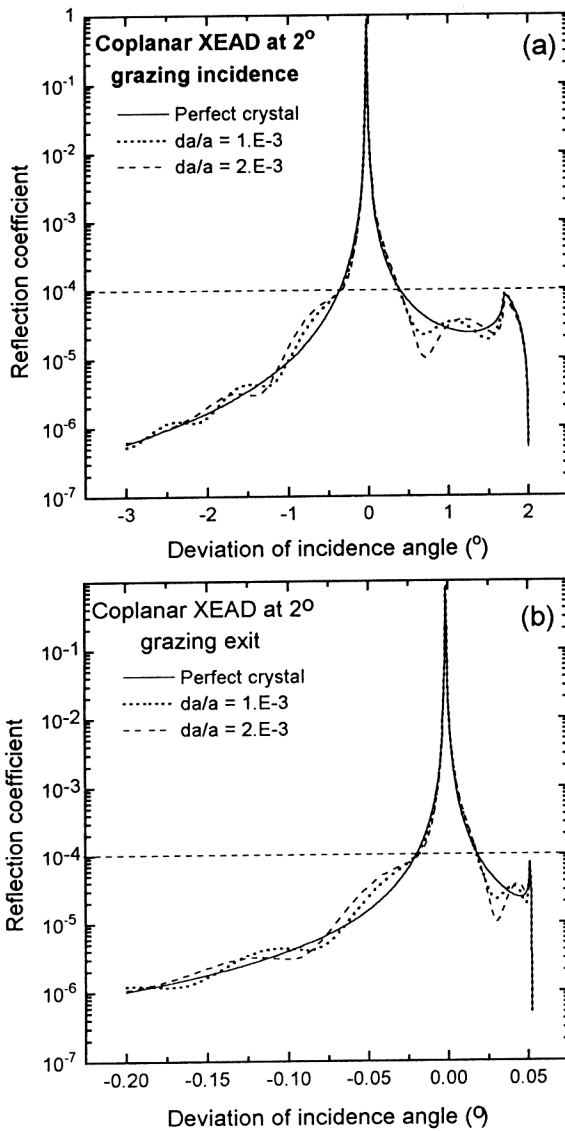


Figure 3. The effect of a 100 Å strained surface layer on coplanar extremely asymmetric x-ray diffraction at 2° grazing incidence (a) and grazing exit (b).

5. Numerical examples and discussion

The diffraction curves with different asymmetry factors γ_0/γ_h were computed with the aim of comparing the change in their shape due to a 100 Å strained layer located on the perfect Ge crystal surface. Computations were carried out for the (220) reflection of σ -polarized x-rays of wavelength $\lambda = 1.54$ Å. The values of $\Delta a_z/a_z$ in the strained layer were assumed to be 1×10^{-3} and 2×10^{-3} .

The computations for the symmetric (220) reflection are presented in figure 2. It can be seen that the effects of the strains are basically displayed far from the Bragg peak at angles where the reflection coefficient is very small: $P_h \leq 2 \times 10^{-5}$. For these values the two-beam x-ray diffraction approximation might be invalid. Therefore, it is doubtful whether the computed effects provide complete correctness. Additionally, due to its small intensity, the effect of the layer measured in the experiment might be overwhelmed by diffuse scattering in the crystal bulk. Thus, the results of the measured

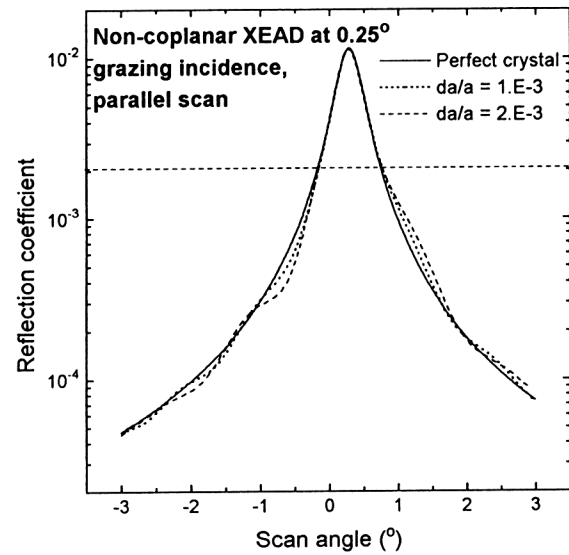


Figure 4. The effect of a 100 Å strained surface layer on non-coplanar extremely asymmetric x-ray diffraction at 0.25° grazing incidence and with a scan retaining the x-ray total external reflection condition.

symmetric Bragg reflection are not supposed to reveal the effects of lattice strain in a 100 Å layer.

Figure 3(a) presents the effects of the same strains on coplanar XEAD with 2° grazing incidence and figure 3(b) the effects for 2° grazing exit. In order to satisfy the coplanar diffraction condition the angle between the plane (110) and the surface was chosen to be 22°. Computations were carried out for the scans along $[\mathbf{k}_0 \times [\mathbf{k}_0 \times \mathbf{n}]]$ which in this case was practically equivalent to the scans along $[\mathbf{k}_0 \times [\mathbf{k}_0 \times \mathbf{h}]]$ and implied variation of the incidence angle. The other scans (along the surface) did not change the Bragg angle and therefore were of no interest with regard to the lattice strain measurements.

It is evident in figure 3 that application of asymmetric geometry produces at least a five-fold enhancement of the strained layer effect, as the curves tails are considerably modified even at $P_h \approx 10^{-4}$. A comparison of figure 3(a) with figure 3(b) shows that the grazing incidence and grazing exit XEAD geometries are equivalent in terms of their sensitivity to lattice strains in thin layers.

All the curves in figure 3 reveal sharp drop down to zero intensity at the right hand tail. In figure 3(a) the curves are subject to dropping because the incidence angle becomes zero or negative. In figure 3(b) this occurs because the exit angle of the diffracted wave turns to an imaginary quantity according to (36). The drops are preceded by local spikes arising from the total external reflection threshold for one of the x-ray wavefields.

Apparently, the maximum sensitivity of XEAD to thin layers can be achieved in those cases in which the Bragg scans maintain the condition of total external reflection. These scans, parallel to the surface, are possible in non-coplanar XEAD. In figure 4 the computations are carried out for non-coplanar XEAD, where the angle between (110) and the surface is 45°, the incident wave strikes the crystal surface at 0.25° and the scans are carried out

along $[k_0 \times n]$, that is, the small incidence angle is kept constant. It can be seen that the strained layer effect is displayed at values of $P_h \simeq 2 \times 10^{-3}$ which is 20 times greater than in the above example. Besides, the effect of strain is already observable at about the 20% level of the Bragg peak, since the maximum value of the reflection coefficient is low. Thus, the sensitivity to strains in thin layers is greatly enhanced.

In conclusion, a theory and an algorithm were developed for computation of XEAD in strained surface multilayers. These techniques can be helpful in planning XEAD experiments and processing XEAD data measured from various thin strained multilayers.

In addition, we would like to note that the effects of surface and interface roughness as well as transition layers in multilayers can be simply added to the proposed model by analogy with what was derived in [20] in neglecting lattice strain.

References

- [1] Batterman B W and Cole H 1964 *Rev. Mod. Phys.* **36** 681
- [2] Afanas'ev A M, Aleksandrov P A and Imamov R M 1986 X-ray structural analysis in studies of single crystals surface layers (Moscow: Nauka) p 48
- [3] Andreeva A M, Borisova S F and Stepanov S A 1986 *Phys. Chem. Mech. Surf.* **4** 951
- [4] Baryshevsky V G 1976 *Sov. Phys. – Appl. Phys. Lett.* **2** 43
- [5] Marra W C, Eisenberger P and Cho A Y 1979 *J. Appl. Phys.* **50** 6927
- [6] Afanas'ev A M and Melkonyan M K 1983 *Acta Cryst. A* **39** 207
- [7] Schurmann H W 1966 *Z. Phys.* **189** 67
- [8] Kishino S and Kohra K 1971 *Japan. J. Appl. Phys.* **10** 551
- [9] Bedynska T 1973 *Phys. Status Solidi a* **19** 365
- [10] Hartwig J 1976 *Phys. Status Solidi a* **37** 417
- [11] Andreeva M A, Rocete K and Khapachev Yu P 1985 *Phys. Status Solidi a* **88** 455
- [11a] Andreeva M A 1986 *Poverkhnost* **10** 15
- [12] Stepanov S A 1994 *Kristallografiya* **39** 221
- [13] Melikyan O G 1991 *Kristallografiya* **36** 549
- [14] Aleksandrov P A and Stepanov S A 1990 *Phys. Chem. Mech. Surf.* **5** 1524
- [15] Aleksandrov P A, Afanas'ev A M and Stepanov S A 1984 *Sov. Phys. – Crystallogr.* **29** 119
- [16] Aleksandrov P A, Afanas'ev A M and Stepanov S A 1984 *Phys. Status Solidi a* **86** 143
- [17] Kaganer V M, Indenbom V L, Vrana M and Chalupa B 1982 *Phys. Status Solidi a* **71** 371
- [18] Afanas'ev A M and Melikyan O G 1990 *Phys. Status Solidi a* **122** 459
- [19] Stepanov S A and Ulianenkov A P 1994 *Acta Cryst. A* **50** at press
- [20] Stepanov S A and Köhler K 1994 *J. Appl. Phys.* submitted